

Article

Search for Novel Phases in Y-Ba-Cu-O Family

Danijel Djurek

Alessandro Volta Applied Ceramics (AVAC), Augusta Šenoje 14, 49247 Zlatar Bistrica, Croatia; danijel@avac.hr

Abstract: In order to search for possible residual minor phases in the Y-Ba-Cu-O family, powdered mixtures of $Y_2O_3 + BaCO_3 + CuO$ and, independently, superconducting compound $YBa_2Cu_3O_{7-x}$ have been treated in evacuated cells and elevated temperatures. $YBa_2Cu_3O_{7-x}$ was reduced to $YBa_2Cu_3O_5$ by use of the special home-designed Taconis–Knudsen vacuum device. Subsequent doping by oxygen converts produced insulator $YBa_2Cu_3O_5$ to semiconductor or metal $YBa_2Cu_3O_{5+x}$ ($0 < x < 0.3$). In addition to $YBa_2Cu_3O_5$, 0.05 volume percent of the minor delafossite phase $Y_2Cu_2O_4$ was spotted in the powder mixture $1/2 Y_2O_3 + 2BaCO_3 + 6Cu_2O$, heated up to $818\text{ }^\circ\text{C}$ in an inert gas atmosphere. An attempt to prepare the insulating bulk delafossite samples was successful, and subsequent doping by oxygen produced novel metallic phases.

Keywords: thermo-acoustic resonator; delafossites; spin-charge separation; spinons; holons

1. Introduction

The discovery of superconductivity (SC) by Chu and co-workers [1] in 1987 in a mixed compound $Y_{1.2}Ba_{0.8}CuO$, indicated by the transition temperature $T_c = 93\text{ K}$, was followed by an announcement [2] suggesting the possible appearance of even higher SC transition temperatures approaching room temperature (RT). Cava and co-workers [3] promoted the formula of the novel superconductor $YBa_2Cu_3O_{7-x}$ (Y-123). The present author and co-workers reported resistive transitions at 210 K, indicated by small diamagnetism [4,5]. The poor reproducibility and stability of the evaluated data were common to worldwide appearances of superconductivity near RT. The probable reason is a very small fraction of the minor phases, which must be traced and recognized in the preparation methodology. The SC transition temperature of $YBa_2Cu_3O_{7-x}$ decreases by removal of oxygen until, for $x > 0.7$, the material becomes an insulator indicated by the tetragonal crystal lattice, and the unit cell dimensions are $a = b = 0.38570\text{ nm}$ and $c = 1.18194\text{ nm}$ [6].

Only little theoretical work has been put forward on the possibility of very high SC transition temperatures. Little promoted an idea [7] on how organic linear chains may obey superconductivity at temperatures higher than the envisaged 30 K, and further concepts published in the scientific literature have operated with quasi-one-dimensional conductivity, since it is evident that Cooper coherence cannot be established at high temperatures in 2D and 3D conducting systems.

Here, the question of the possibility of lower oxidation states in Y-123, say $1 < x < 2$, arises, while the crystal structure could be isomorphic with the original tetragonal phase. This paper describes a preparation of the novel metal $YBa_2Cu_3O_{5+x}$ (Y-5). In addition to Y-5, the next minor phase $YCuO_2$ is found in Y-Ba-Cu-O mixtures, and its structural, resistive and magnetic properties are reviewed.

2. Experimental Section

In order to trace the low concentrated minor phases in the Y-Ba-Cu-O family, the standard preparations of Y-123 in the flowing oxygen atmosphere at $935\text{ }^\circ\text{C}$ must be replaced by more unconventional methods, which include treatment in an evacuated cell and firing temperatures ranging from $500\text{--}1100\text{ }^\circ\text{C}$. The powders of prepared compounds



Citation: Djurek, D. Search for Novel Phases in Y-Ba-Cu-O Family. *Condens. Matter* **2024**, *9*, 10. <https://doi.org/10.3390/condmat9010010>

Academic Editor: Andrzej M. Oleś

Received: 17 October 2023

Revised: 12 December 2023

Accepted: 20 December 2023

Published: 17 January 2024



Copyright: © 2024 by the author. Licensee MDPI, Basel, Switzerland. This article is an open access article distributed under the terms and conditions of the Creative Commons Attribution (CC BY) license (<https://creativecommons.org/licenses/by/4.0/>).

were pressed into pellets measuring 8 mm in diameter and 0.8–1 mm in thickness, and in order to measure electric resistance, we pressed together four gold wires, 100 microns in diameter, with the powder.

2.1. $YBa_2Cu_3O_{5+x}$

Two oxygen atoms were removed from the Y-123 ($x = 0.16$) pellet by use of the vacuum sublimation device designed in this laboratory and schematically presented in Figure 1.

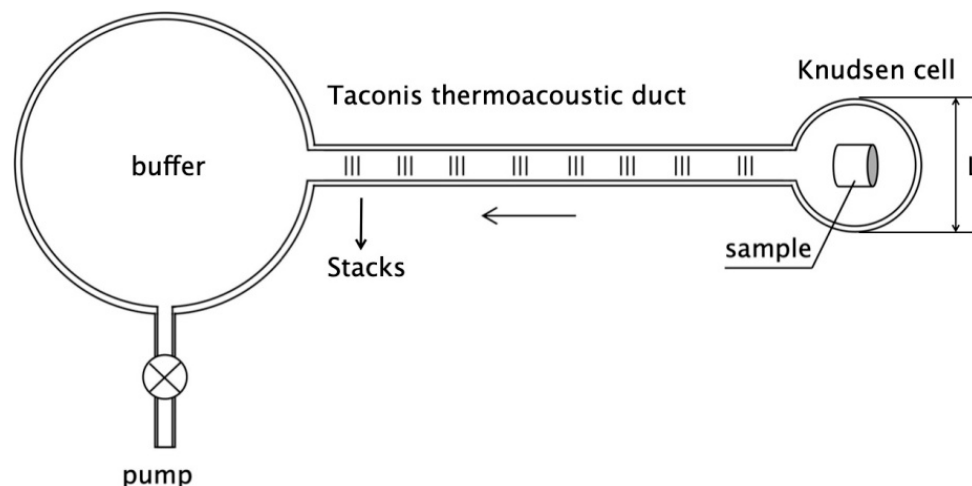


Figure 1. Principle of a thermo-acoustic resonator that resonates between Taconis thermo-acoustic duct and Knudsen cell. Arrows show the formation of the thermoacoustic stacks.

The thermo-acoustic engine resonates between the Taconis thermo-acoustic duct [8] and Knudsen cell, the latter held at 645 °C, while the buffer is at RT. Gas dynamics in a Taconis duct is governed by two parameters: the dynamic gas viscosity $\nu = \mu/\rho$, indicated by a viscous depth $l = (2\nu/\omega)^{1/2}$, and thermal diffusivity of the gas in the duct, given by $k = \lambda/\rho \cdot c_p \cdot \lambda$, c_p and ρ are the thermal conductivity, specific heat and gas density, respectively. The ratio of a dynamic viscosity and thermal diffusivity defines the Prandtl number governing the sublimation efficiency of the sample. The Taconis gas density stacks are visualized in the duct.

The practical performance of the thermo-acoustic resonator is visualised in Figure 2. The sample is positioned in the cell 1, and the pumping was proceeded through screw thread 2, funnelled to a coaxial duct between sample holder 3 and outer tube 4. The diameters between the outer tube 4 and inner sample holder 3 differ by 0.14 mm and define the cross-section of the duct. The volume of the Knudsen cell is 0.8 cm³, and it resonates with Taconis oscillations, giving rise to pressure fluctuations strong enough to drain oxygen from the sample. Obviously, molecular velocities $v = (2\delta p/\rho)^{1/2}$, driven by pressure oscillations in a small density range δp , are in the supersonic regime, indicating that strong sublimation occurs. The pumping path in the coaxial duct terminates in a vacuum buffer, and the dynamic pressure of ~0.15 mbar in the buffer was adjusted by a fine needle valve. The temperature was monitored by use of the type K thermocouple 5. An additional adjusting parameter is provided by the fraction of the Taconis coaxial duct exposed to the hot zone of the oven. The Knudsen cell was maintained at a constant temperature of 645 °C, and enhanced pressure oscillations in the cavity favoured a strong reduction of oxides. For instance, copper oxide CuO was reduced to pure copper at already 332 °C. The resonant frequency of 11.2 kHz was measured by use of a hot wire anemometer 6 assembled from a platinum wire measuring 25 microns in diameter and fixed in the buffer interior.

The reduction of the Y-123 superconductor was monitored by weight, and XRD data are presented in Figure 3. Refinement provides the dimensions of the tetragonal cell: $a = b = 0.38605$ nm and $c = 1.18450$ nm. The samples are indicated by yellow colour,

and an additional evaluation of the oxygen content was performed by a reduction in hydrogen atmosphere. The final result was $\text{YBa}_2\text{Cu}_3\text{O}_{5\pm 0.06}$. When exposed to free air atmosphere, Y-5 absorbs the oxygen, and, in the course of one month of exposure, it converts to $\text{YBa}_2\text{Cu}_3\text{O}_{5.14}$.

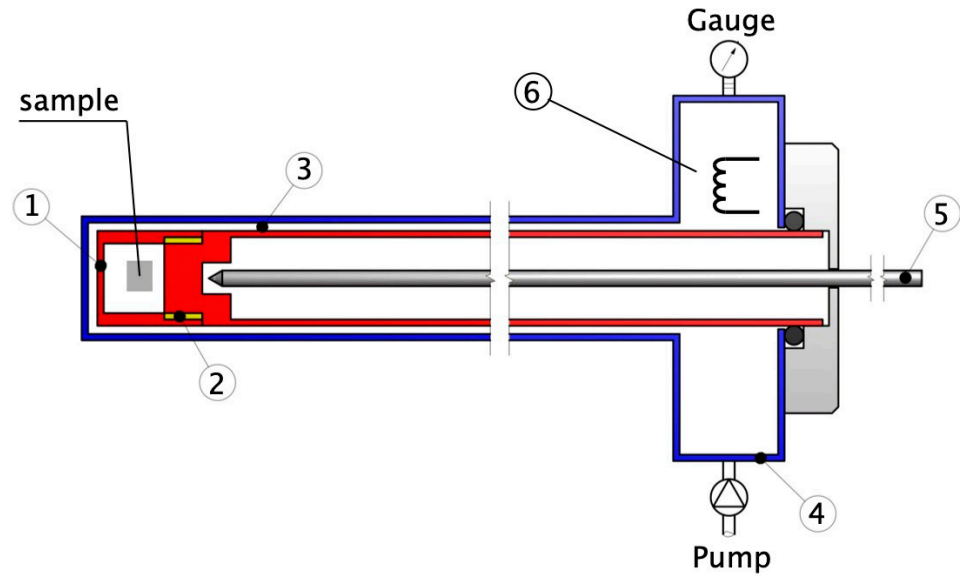


Figure 2. Technical performance of the thermo-acoustic resonator.

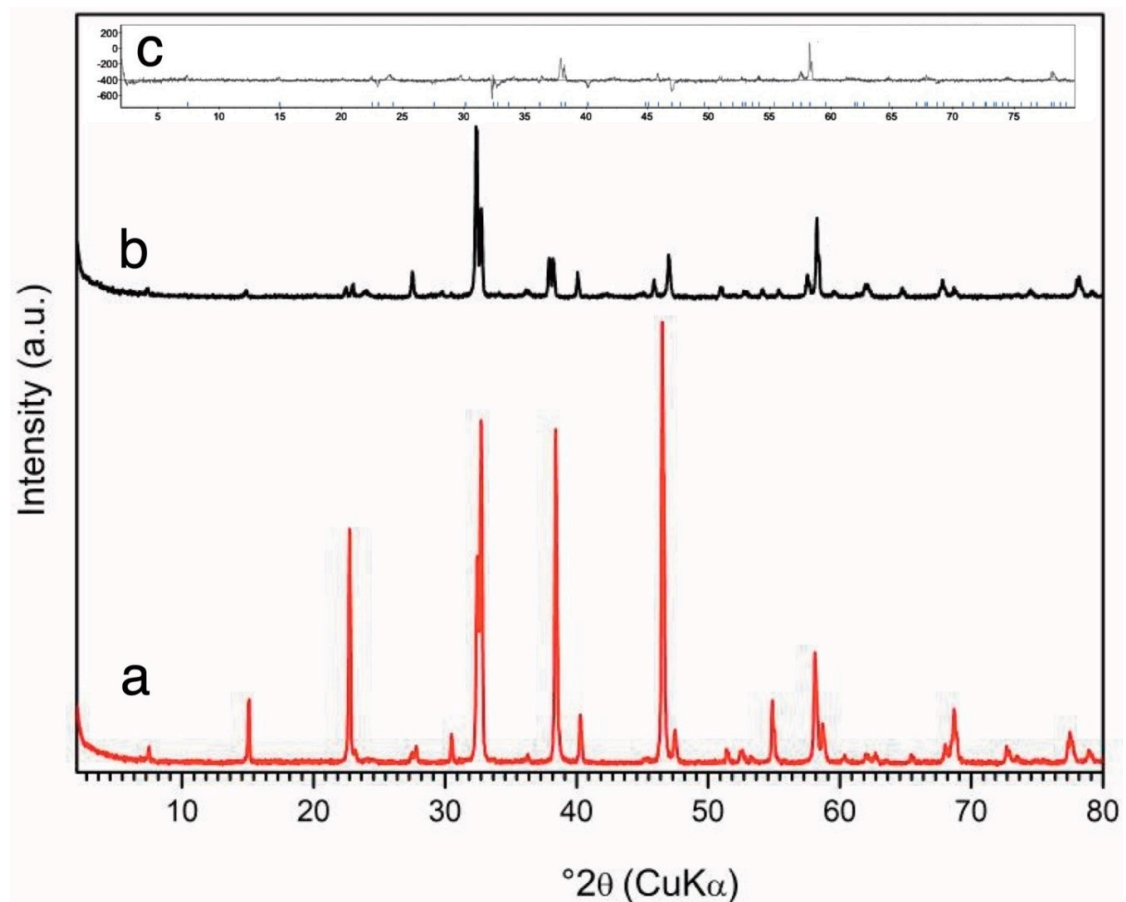


Figure 3. X-ray diffractograms: (a) the superconducting sample Y-123, (b) $\text{YBa}_2\text{Cu}_3\text{O}_5$ (Y-5) obtained by removal of two oxygen atoms from the same sample Y-123, and (c) Y-5 structure refinement.

Doping of the pellet $\text{YBa}_2\text{Cu}_3\text{O}_5$ by oxygen proceeded in a calibrated alumina cell. In an independent heating stage, the cell was filled with argon gas in order to evaluate an increase of the pressure by heating and to trace the possible degassing from the ceramic background. Oxygen pressure was measured by use of an absolute capacitance gauge with a sensitivity better than 0.1 mbar.

The oxygen doping is presented in Figure 4, and the starting oxygen pressure at RT was 50 mbar (a). The attached straight line shows an increase of the pressure as a result of the cell heating, prior to absorption which starts at 292 °C. It is indicative that the slope of the temperature-dependent pressure after absorption differs from the initial one and that an additional absorption step is visible at 632 °C, appealing for a second minor phase in Y-5. The release of adsorbed oxygen starts at 825 °C, and additional pressure above the linear straight line results from the partial deterioration of the unit cell Y-5. The temperature dependence of the oxygen pressure by cooling to RT is shown in curve (b), while the yellow pellet becomes black. The final oxygen content of 2.625 moles in the pellet was evaluated by weight and by reduction in a 2 bar hydrogen atmosphere at 410 °C.

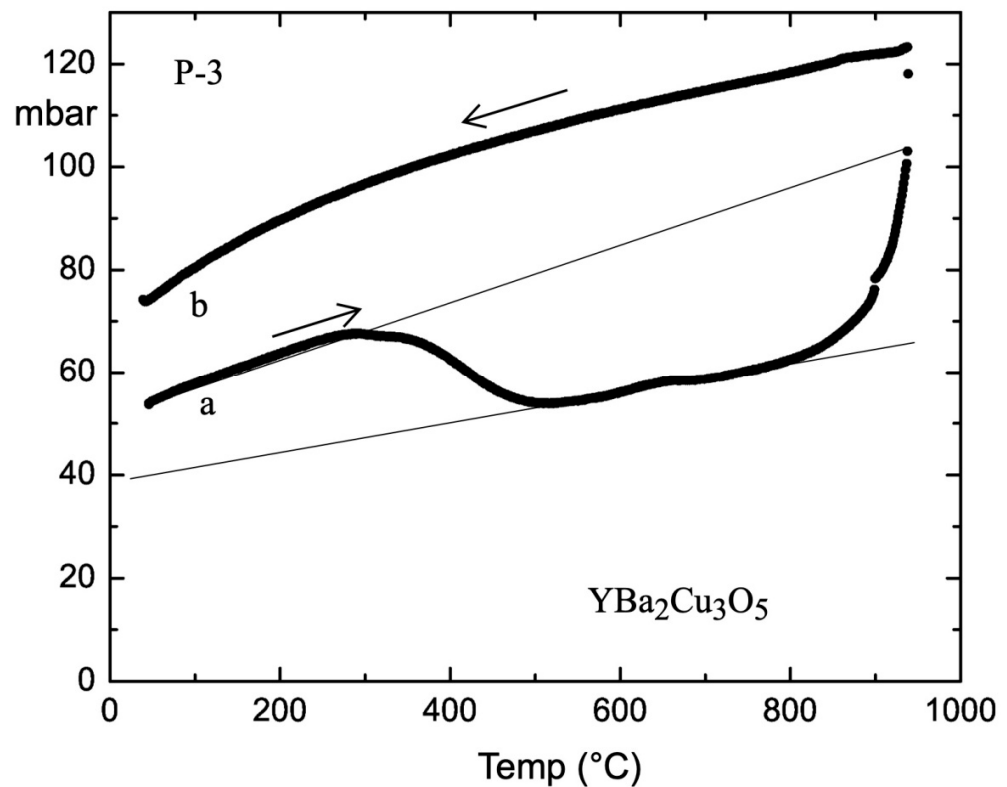


Figure 4. Temperature dependence of the oxygen pressure in the cell containing the pellet of $\text{YBa}_2\text{Cu}_3\text{O}_5$; (a) heating stage symbolised by arrow, (b) cooling stage symbolised by arrow.

In the next preparation, $\text{YBa}_2\text{Cu}_3\text{O}_{5.32}$ was produced, and the temperature dependence of the resistance, measured in 10 mA AC current 20 Hz by use of a lock-in amplifier, is shown in Figure 5. It falls down at 41 °C, and a magnified portion between -10 and $+10$ °C is shown in the inset. Amplification of the lock-in transformer is frequency-dependent for very small resistances that are measured, and a silver pellet of a similar size was used as an etalon for frequency calibration of the transformer. A comparatively high measuring current lifts the sample resistivity to 10^{-5} Ωcm , while the application of 1 mA results in a resistivity under 10^{-6} Ωcm . Extrapolation to zero current gives $0.17 \cdot 10^{-6}$ Ωcm at the ice point.

In the next preparation, $\text{YBa}_2\text{Cu}_3\text{O}_{5.32}$ was produced, and the temperature dependence of the resistance, measured in 10 mA AC current 20 Hz by use of a lock-in amplifier, is shown in Figure 5. It falls down at 41 °C, and a magnified portion between -10 and $+10$ °C

is shown in the inset. Amplification of the lock-in transformer is frequency-dependent for very small resistances that are measured, and a silver pellet of a similar size was used as an etalon for frequency calibration of the transformer. A comparatively high measuring current lifts the sample resistivity to $10^{-5} \Omega\text{cm}$, while the application of 1 mA results in a resistivity under $10^{-6} \Omega\text{cm}$. Extrapolation to zero current gives $0.17 \times 10^{-6} \Omega\text{cm}$ at the ice point.

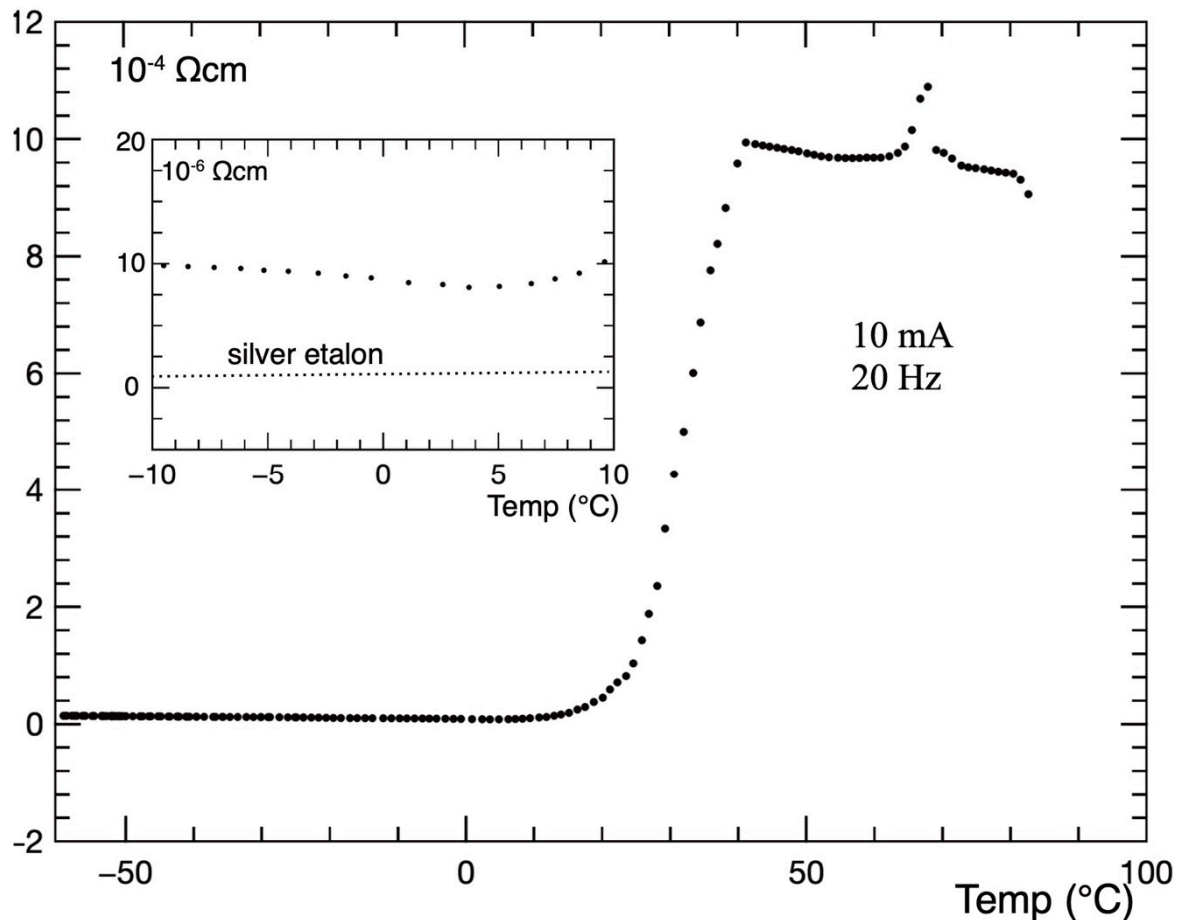


Figure 5. Temperature dependence of the electric resistance of $\text{YBa}_2\text{Cu}_3\text{O}_{5.32}$ measured at 20 Hz and 10 mA by lock-in amplifier. Inset shows the magnified data in the temperature range $-10^\circ\text{C} + 10^\circ\text{C}$.

The measurement of the AC magnetic susceptibility of $\text{YBa}_2\text{Cu}_3\text{O}_{5.25}$ was performed by use of a high-resolution CryoBIND Research susceptometer. The real (black) and imaginary (red) parts are shown in Figure 6. The mass of the sample was 57 mg. The AC field was 0.75 Oe (RMS), the frequency was 231 Hz, and the superimposed DC field was 44 Oe. The data appear for two diamagnetic phases. One phase is indicated by a temperature-dependent susceptibility decreasing by cooling from $+11^\circ\text{C}$, and its volume fraction is estimated to be 0.05 percent. The second phase is $\text{YBa}_2\text{Cu}_3\text{O}_{7-x}$ that remained after incomplete draining in the Knudsen cell, and its volume fraction is 0.25 percent.

An important achievement of these experiments is, in contrast to past decades events, a fair reproducibility of the measured data. However, an appreciable increase of the diamagnetic fraction was not observed during the preparation, and this in turn calls attention to the fact that the yellow phase may not be a carrier of diamagnetic susceptibility above 93 K. Moreover, although XRD stressed the iso-structural properties of the tetragonal $\text{YBa}_2\text{Cu}_3\text{O}_6$, shown in Figure 3, several additional and indicative diffractions seem to appear.

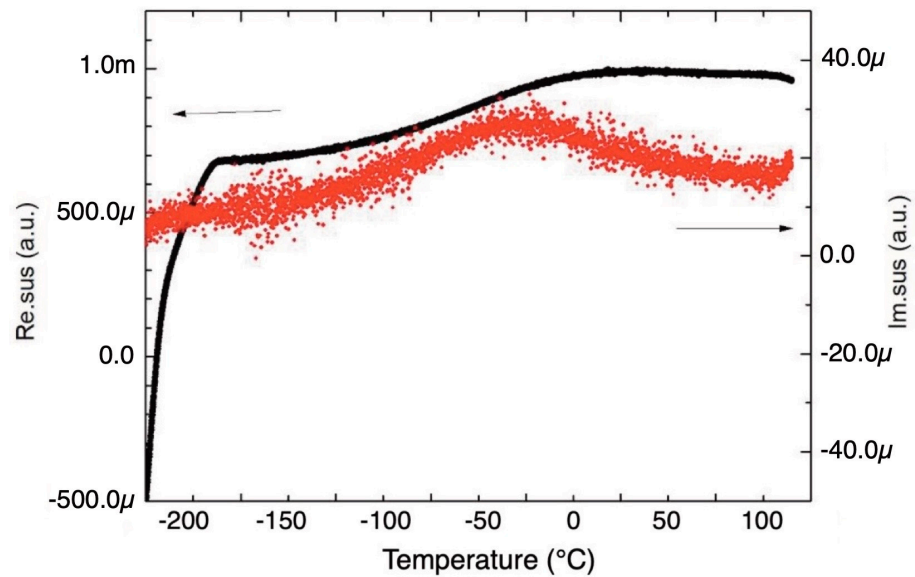


Figure 6. Temperature dependence of the real (black) and imaginary (red) part of the AC susceptibility of the oxygen-doped $\text{YBa}_2\text{Cu}_3\text{O}_{5.25}$; 0.25 volume percent of superconducting Y-123 is visible left of the black curve, remaining after thermo-acoustic reduction.

2.2. Delafossite $\text{Y}_2\text{Cu}_2\text{O}_{4+\delta}$

The non-reacted mixture Y-123 was heated and analyzed by simultaneous differential scanning calorimeter (DSC) and thermogravimetry (DTG) in an inert gas atmosphere. The measured data, shown in Figure 7, stress endothermic features at 818 °C, 926 °C (Y-123 phase), 1028 °C (green phase Y_2BaCuO_5), and 1175 °C. The endothermic peak at 818 °C is indicated by the absence of BaCO_3 decomposition. Obviously, a reaction involves no barium, which sounds like the group of oxides $\text{Y}^n\text{Cu}^n\text{O}_x$ referred in the literature to as delafossites. The lowest member is hexagonal YCuO_2 , first synthesized by Ishiguro and co-workers [9] and later examined by Aride and co-workers [10].

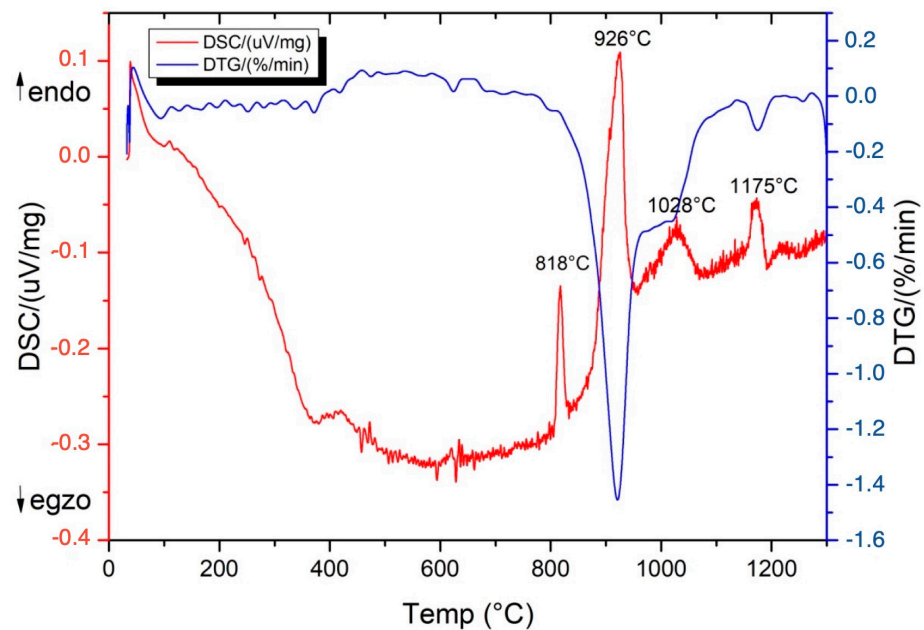


Figure 7. DSC-DTG record of the previously unfired mixture $1/2\text{Y}_2\text{O}_3 + 2\text{BaCO}_3 + \text{Cu}_2\text{O}$ in argon atmosphere. Endothermic feature at 926 °C corresponds to formation of the tetragonal Y-123 phase.

The starting powder components for the preparation of $\text{Y}_2\text{Cu}_2\text{O}_4$ are $\text{Y}_2\text{O}_3 + \text{Cu}_2\text{O}$, pressed in pellets and fired for 24 h in vacuum at 818–820 °C. The pink-coloured pellet

becomes reddish-black and insulating, while the XRD record confirms the presence of $YCuO_2$, non-reacted Y_2O_3 and elementary Cu. Preparations at 0.5 and 1 bar oxygen result in reddish and green/grey colours, respectively, both species being insulators. Lattice parameters of the hexagonal cell are $a = 0.35206$ nm and $c = 1.1418$ nm.

The next experiments were focused on the insulating samples $Y_2Cu_2O_4$ doped by comparatively small oxygen pressures. Figure 8a,b show a gradual decrease of the resistivity, measured in air, with increasing oxygen pressure in the reaction cell. Inset of Figure 8a presents the structure of the pellet prepared for the measurement of the electric resistivity. The pronounced maxima of resistivities are observed at -21 °C and -53 °C for oxygen pressures of 2.4 and 10.2 mbar, respectively.

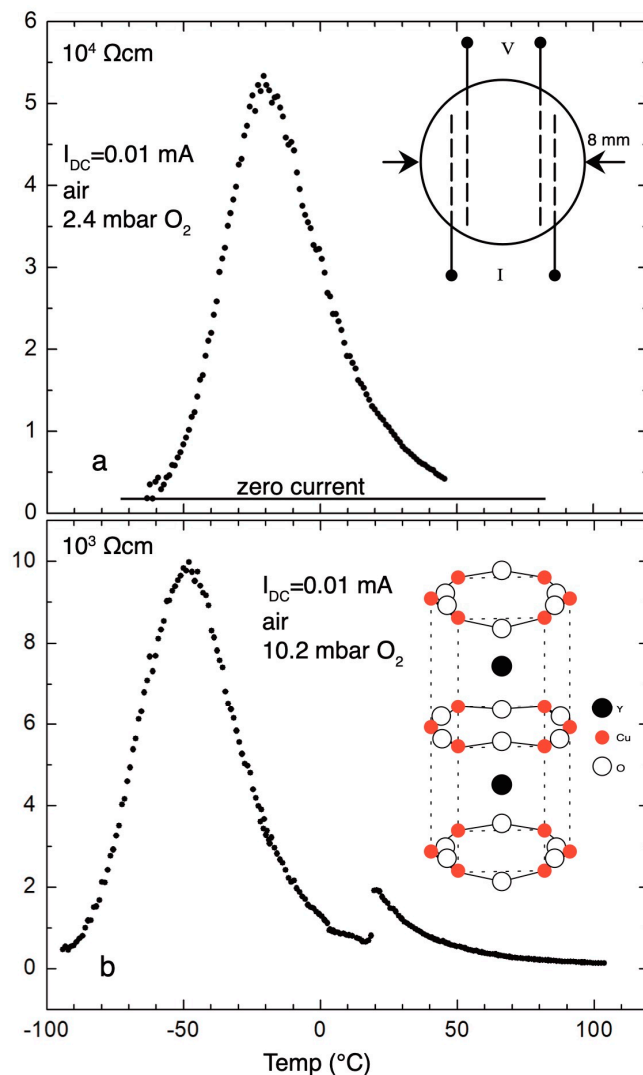


Figure 8. Temperature dependence of the resistivity of $Y_2Cu_2O_4$, measured in air, after annealing in oxygen atmosphere: (a) 2.4 mbar, and inset shows the sample pellet with impressed 100 micron gold wires; (b) 10.2 mbar.

It was observed that annealing near 40–50 mbar oxygen results in the lowest resistivities, in the order of $10^{-4} \Omega cm$ at the ice point, and by further increase of the oxygen pressure, higher than 150 mbar, samples gradually become insulators again. In both extreme cases, the valency of copper is uniform: Cu^+ in zero pressure annealing and Cu^{2+} in 1 bar. The mixed valency state Cu^+/Cu^{2+} , as a precondition for conductivity, is established for oxygen pressures between 0.01 and 0.5 bar. Depending on the annealing pressure, pellets are differently coloured, which appeals for the more complex pressure-temperature phase diagram.

The next doping pressure, dependent on temperature, is shown in Figure 9. The starting pressure at RT was 100 mbar. In order to minimize the background increase of the pressure due to the heating, the pressure cell was externally buffered. The absorption starts at 395 °C and finishes at 587 °C. In order to eliminate the contribution of the oxygen that adhered on the grain boundaries, the pressure cell was evacuated prior to cooling to RT, and an increase of the released oxygen was visible at temperatures approaching RT. The remaining oxygen pressure in the air was 38 mbar, also confirmed by a weight control.

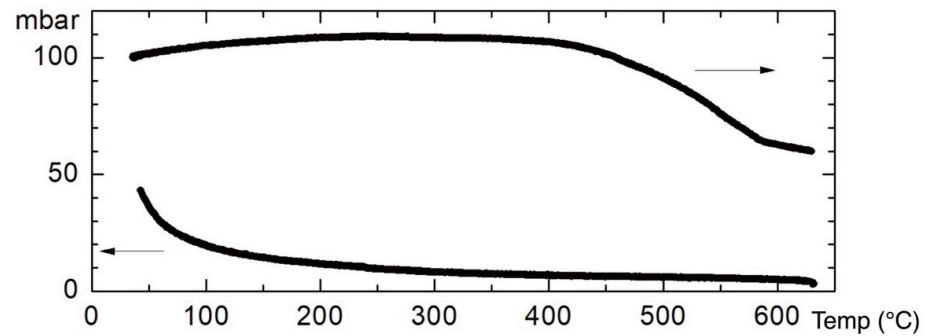


Figure 9. Doping of $\text{Y}_2\text{Cu}_2\text{O}_4$ by oxygen and cooling to RT after evacuation. Right and left arrow mark heating and cooling stage respectively.

Figure 10 shows the temperature dependence of the electric resistivity measured in air, after annealing in oxygen at temperatures up to 645 °C, as presented in Figure 9; it decreases comparatively slow by cooling, due to the high measuring current of 10 mA. Resistivity falls below $10^{-6} \Omega\text{cm}$ at a temperature of less than -100°C .

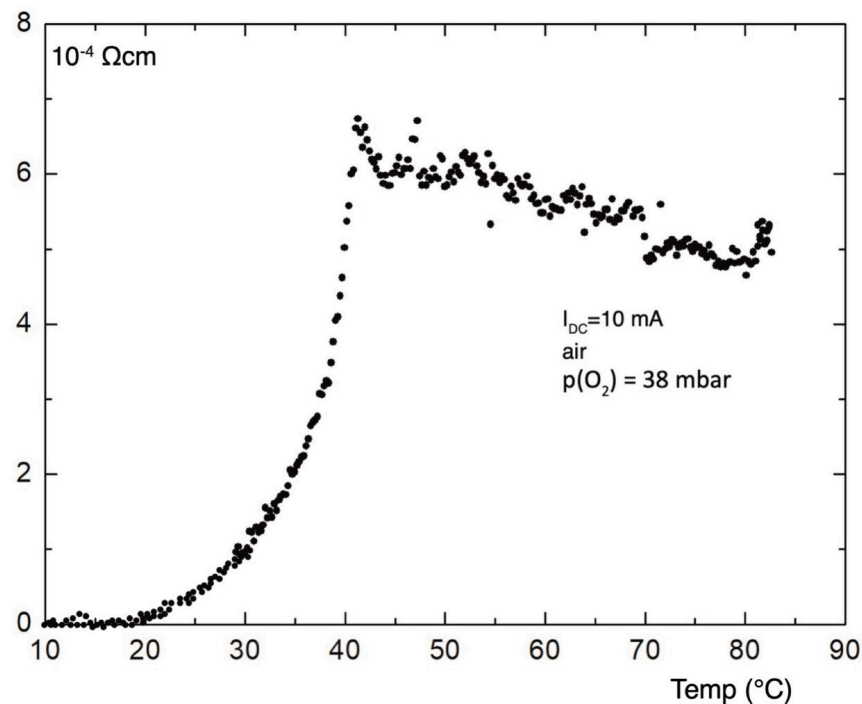


Figure 10. Temperature dependence of the resistivity, measured in air, of the sample $\text{Y}_2\text{Cu}_2\text{O}_4$ after annealing in 38 mbar oxygen atmosphere at 645 °C.

The AC magnetic susceptibility of the pellet presented by resistivity, shown in Figure 10, was measured in air by use of a primary and two secondary coaxial coils. The signal from the two secondary coils was compensated when both were empty. A certified pellet of High Tc superconductor $\text{GdBa}_2\text{Cu}_3\text{O}_{7-x}$, with a diameter of 10 mm and thickness

of 1 mm, was used as an etalon. The temperature dependence of AC susceptibility is shown in Figure 11.

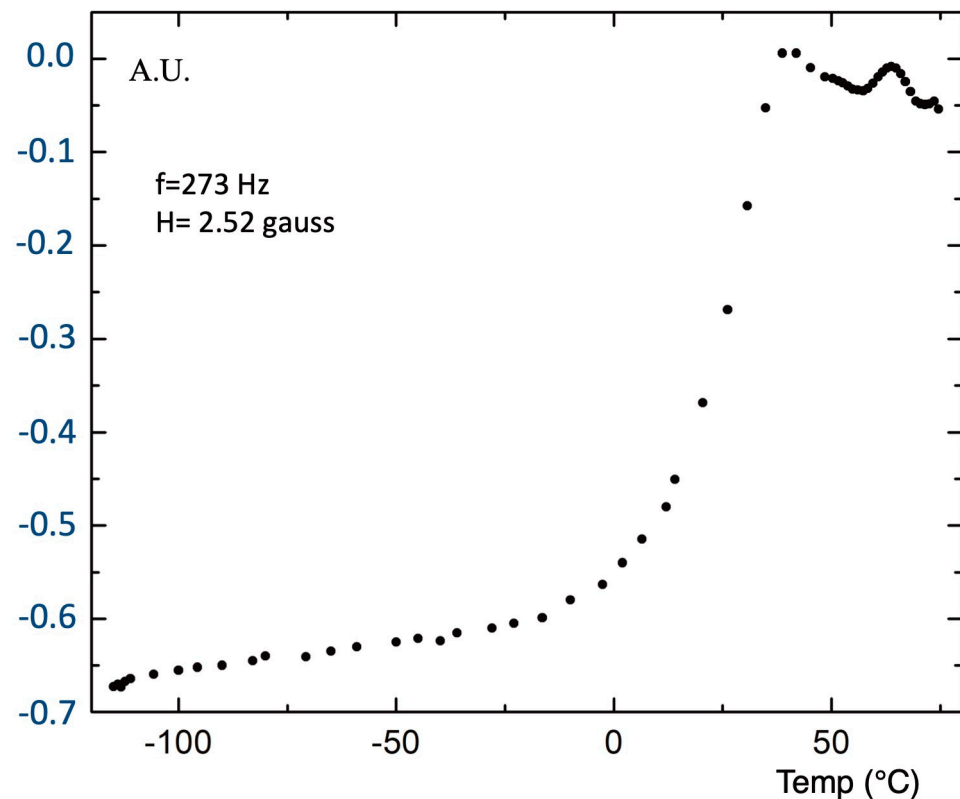


Figure 11. Temperature dependence of magnetic AC susceptibility of the pellet $Y_2Cu_2O_{4+\delta}$ used in electric resistance measurement and shown in Figure 10. Pellet was fixed in a secondary coil balanced with another identical coil in secondary circuit.

3. Discussion

Two compounds, $YBa_2Cu_3O_5$ and $Y_2Cu_2O_4$, are insulators containing only Cu^+ cations embedded in mutually orthogonal Cu^+-O-Cu^+ chains. The absorption of oxygen partly converts Cu^+ to Cu^{2+} , creating a mixed valency state indicated by the good conductivity of electricity proceeding along the polarized chains, which is followed by transitions to a low resistivity state near RT. The question arises why the diamagnetic contribution in the predominant mono-phase Y-5, presented in Figure 6, is still small. It seems more likely that it arises from $Y_2Cu_2O_{4+\delta}$ as a minor phase in Y-5. However, the premature exclusion of resistive and magnetic transitions in Y-5 does not seem productive, since relatively high amount of absorbed oxygen suggests a promising set of novel experiments.

In some respects, insulating $Y_2Cu_2O_4$ is similar to La_2CuO_4 , which becomes superconducting when doped by oxygen [11–13], and both oxides are very sensitive on doping level δ . Even a small exposure to oxygen reduces dramatically the electric resistivity, as shown in Figure 8. A pronounced maximum of the temperature-dependent resistivity reflects the competition of magnetic (spinon) and electric (holon) degrees of freedom expressed in the $t - J$ Hamiltonian involved in modern models of spin-charge separation. In classic theories of superconductivity, such as BCS, Cooper instability drives the electron pairing at temperature T^* : $\ln(kT^*/p_F v_s) = -p_F \cdot v_s / J$. p_F and v_s are the Fermi surface momentum and spin velocity, respectively. At higher doping densities, the spinon and holon velocities are equal, $v_h = v_s = J/p_F$, and the maximum of the temperature-dependent resistivity occurs at $kT^* = J$. J is linear-dependent on small doping δ [14], and the expression of the Cooper instability explains maxima in Figure 8.

Spin-charge separation was first observed in a one-dimensional compound $SrCuO_2$ [15,16]. Cu-O distances in $Y_2Cu_2O_4$ are 3.52 Å, which is considerably higher

than those in insulating SrCuO₂ (0.16 nm) and Y-5 (0.193 nm). Consequently, spinon and holon velocities will be higher at a smaller Cu-O chain density [17], which is followed by a smaller charge transfer gap. Spin-charge separation embodied in the $t - J$ Hamiltonian indicates a strong competition between the superconductivity and insulating state. Competition is the usual guide, as a familiar method, in the search for new superconductors involving insulators as possible candidates. SrCuO₂ is not superconducting, indicating that a more complicated connection between superconductivity and spin charge separation must be considered. In order to put forward further analyses, it may be studied SrCuO₂ partly reduced in the above described thermo-acoustic resonator which in turn induces a mixed valency state.

4. Conclusions

Two insulating phases, YBa₂Cu₃O₅ and Y₂Cu₂O₄, which appear as minor components in the preparation of the YBa₂Cu₃O_{7-x} superconductor, were focused and independently prepared. Doping of Y₂Cu₂O₄ by oxygen results in a one-dimensional conductor, indicating that some resistive and magnetic properties call attention to a novel superconductivity.

Funding: This research received no external funding.

Data Availability Statement: Data are available on the request.

Acknowledgments: The author is grateful to Mladen Prester and Gjuro Drobac (CryoBIND Research d.o.o.) for the high-resolution AC susceptibility measurement presented in Figure 6. The author profited from discussions with Matej Ercegović (Faculty of Chemical Engineering and Technology–FKIT, Zagreb).

Conflicts of Interest: Danijel Djurek was employed by the company Alessandro Volta Applied Ceramics. He declare that the research was conducted in the absence of any commercial or financial relationships that could be construed as a potential conflict of interest.

References

1. Wu, M.K.; Ashburn, J.R.; Torng, C.J.; Hor, P.H.; Meng, R.L.; Gao, L.; Huang, Z.J.; Wang, Y.Q.; Chu, C.W. Superconductivity at 93 K in a new mixed-phase Y-Ba-Cu-O compound system at ambient pressure. *Phys. Rev. Lett.* **1987**, *58*, 908–910. [[CrossRef](#)] [[PubMed](#)]
2. Chu, C.W. NSF news release. *New York Times*, 10 March 1987.
3. Cava, R.J.; Batlogg, B.; van Dover, R.B.; Murphy, D.W.; Sunshine, S.; Siegrist, T.; Remeika, J.P.; Rietman, E.A.; Zahurak, S.; Espinosa, G.P. Bulk Superconductivity at 91 K in Single-Phase Oxygen-Deficient Perovskite Ba₂YCu₃O_{9-δ}. *Phys. Rev. Lett.* **1987**, *58*, 1676–1679. [[CrossRef](#)] [[PubMed](#)]
4. Djurek, D.; Prester, M.; Knezović, S.; Drobac, D.; Milat, O. Low Resistance State up to 210 K in a Mixed Compound Y-Ba-Cu-O. *Phys. Lett. A* **1987**, *123*, 481–484. [[CrossRef](#)]
5. Djurek, D.; Prester, M.; Knezović, S.; Drobac, D.; Milat, O.; Babić, E.; Brničević, N.; Furić, K.; Medunić, Z.; Vukelja, T. Possible Superconducting State up to 210 K in the New Composition of Y-Ba-Cu-O. *Croat. Chem. Acta* **1987**, *60*, 351–352.
6. Banerjee, S.; Dasgupta, C.; Mukerjee, S.; Ramakrishnan, T.V.; Sarkar, G. High temperature superconductivity in the cuprates: Materials, phenomena and a mechanism. In Proceedings of the AIP Conference Proceedings 2018, Berhampur, Odisha, India, 19–21 December 2017; Volume 2005, p. 020001. [[CrossRef](#)]
7. WLittle, A. Possibility of Synthesizing an Organic Superconductor. *Phys. Rev.* **1964**, *134*, A1416–A1424. [[CrossRef](#)]
8. Taconis, K.W.; Beenakker, J.J.; Nier, A.O.C.; Aldrich, L.T. Measurements concerning the vapour-liquid equilibrium of solutions of He³ in He⁴ below 2, 19 K. *Physica* **1949**, *15*, 733–739. [[CrossRef](#)]
9. Ishiguro, T.; Ishizawa, N.; Mizutani, N.; Kato, M. A New Delafossite-Type Compound CuYO₂. *J. Solid State Chem.* **1983**, *49*, 232–236. [[CrossRef](#)]
10. Aride, J.; Flandrois, S.; Taibi, M.; Boukhari, A.; Drillon, M.; Soubeyroux, J.L. New Investigations on Magnetic and Neutron Diffraction Properties of Y₂Cu₂O₅. *Solid State Commun.* **1989**, *72*, 459–463. [[CrossRef](#)]
11. Chaillout, C. Structural and Physical Properties of Superconducting La₂CuO_{4+δ} Materials and Crystallographic Aspects of HT_c-Superconductivity. *NATO ASI Ser.* **1994**, *263*, 129–144.
12. Beille, J.; Cabanel, R.; Chaillout, C.; Chevalier, B.; Demazeau, G.; Deslandes, F.; Ettourmeau, J.; Leja, P.; Michel, C.; Provost, J.; et al. Superconductivity of La₂Cu_xO_{4-y}. *C. R. Acad. Sci. Paris* **1987**, *304*, 1097–1112. [[CrossRef](#)]
13. Grant, P.M.; Parkin, S.S.P.; Engler, V.Y.L.E.M.; Ramirez, M.L.; Vazquez, J.E.; Lim, G.; Jakowitz, R.D.; Greene, R.L. Evidence for superconductivity in La₂CuO₄. *Phys. Rev. Lett.* **1987**, *58*, 2482–2487. [[CrossRef](#)] [[PubMed](#)]
14. Anderson, P.W. Experimental Constraints on the Theory of High-Tc Superconductivity. *Science* **1992**, *256*, 1526–1531. [[CrossRef](#)] [[PubMed](#)]

15. Kim, C.; Matsuura, A.Y.; Shen, Z.-X.; Motoyama, N.; Eisaki, H.; Tohuyama, S.U.T.; Maekava, S. Observation of Spin-Charge Separation in One-Dimensional SrCuO₂. *Phys. Rev. Lett.* **1996**, *77*, 4054–4057. [[CrossRef](#)] [[PubMed](#)]
16. Kim, B.J.; Koh, H.; Rotenberg, E.; Oh, S.-J.; Eisaki, H.; Motoyama, N.; Uchida, S.; Tohoyama, T.; Shen, S.M.Z.-K.; Kim, C. Distinct spinon and holon dispersions in photoemission spectral functions from one-dimensional SrCuO₂. *Nat. Phys.* **2006**, *2*, 397–401. [[CrossRef](#)]
17. Senaratne, R.; Cavazos-Cavazos, D.; Wang, S.; He, F.; Chang, Y.T.; Kafle, A.; Pu, H.; Guan, X.W.; Hulet, R.G. Spin-Charge separation in a one-dimensional Fermi gas with tunable interactions. *Science* **2022**, *376*, 1305–1332. [[CrossRef](#)] [[PubMed](#)]

Disclaimer/Publisher’s Note: The statements, opinions and data contained in all publications are solely those of the individual author(s) and contributor(s) and not of MDPI and/or the editor(s). MDPI and/or the editor(s) disclaim responsibility for any injury to people or property resulting from any ideas, methods, instructions or products referred to in the content.